Journal of Magnetism and Magnetic Materials 116 (1992) 375–385
North-Holland

Crystal and magnetic structure of TbNiGe and DyNiGe compounds

G. André [a], F. Bourée [a], M. Kolenda [b], A. Oleś [c], A. Pacyna [d], M. Pinot [a], W. Sikora [c] and A. Szytuła [b]

[a] *Laboratoire Léon Brillouin (CEA–CNRS), CEN-Saclay, 91191 Gif-sur-Yvette Cedex, France*
[b] *Institute of Physics, Jagellonian University, Reymonta 4, 30-059 Cracow, Poland*
[c] *Department of Physics and Nuclear Technology, Academy of Mining and Metallurgy, 30-059 Cracow, Poland*
[d] *Institute of Nuclear Physics, Radzikowskiego 152, 31-342 Cracow, Poland*

Received 11 March 1992; in revised form 6 April 1992

The results of X-ray, neutron diffraction and magnetometric measurements for TbNiGe and DyNiGe compounds are presented. Both compounds crystallize in an orthorhombic TiNiSi-type crystal structure and are antiferromagnets with Néel temperature of 18 and 6 K, respectively. At low temperatures both compounds have square modulated structures with a wave vector $\boldsymbol{k} = (\frac{2}{3}, \frac{1}{3}, 0)$. With increase in temperature a change to a sinusoidally modulated structure for TbNiGe and probably a cycloidal spiral structure for DyNiGe is observed. In both structures and both phases the magnetic moments are parallel to the *c*-axis. In the case of the TbNiGe compound a coexistence of two magnetic structures over a wide temperature range is observed. The experimentally determined magnetic structures are in agreement with those proposed by symmetry analysis.

1. Introduction

A large number of equiatomic ternary rare-earth intermetallic compounds with the general formula RTX (R – rare earth, T – transition element, and X – In, Si, Sn, Ga or Ge) are known to exist [1–3]. They crystallize in several different types of structures [3–5]. X-ray diffraction data indicate that RNiGe compounds crystallize in an orthorhombic structure [6].

From magnetometric measurements it follows that the compounds with Gd, Tb, Dy and Er are antiferromagnets and the Néel temperatures are 11, 7, 9 and 6 K, respectively [6].

In this work we present results of X-ray and neutron diffraction as well as magnetometric measurements undertaken in order to determine the crystal and magnetic structure of TbNiGe and DyNiGe.

Correspondence to: Prof. A. Szytuła, Institute of Physics, Jagellonian University, 30-059 Cracow, Reymonta 4, Poland.

2. Experimental

The TbNiGe and DyNiGe sample were synthesized by arc melting of stoichiometric amounts of high-purity components. The samples were subsequently annealed in vacuum for 100 h at 1073 K.

X-ray diffraction patterns of TbNiGe and DyNiGe compounds consisted of a large number of lines characteristic for an orthorhombic crystal structures. The lattice constants determined, are in a good agreement with those in ref. [6].

The magnetometric measurements were carried out using an RH Cahn balance in the temperature range from 4.2 to 300 K.

Neutron diffraction data were obtained by means of the neutron powder diffractometer G4.1

and 3T2 installed at the Orphée reactor (Laboratoire Léon Brillouin, Saclay) with an incident neutron wavelength of 2.426 and 1.2268 Å. Neutron scattering lengths were taken from the Delapalme work [7] and the Tb^{3+} and Dy^{3+} form factors were taken from the Freeman and Desclaux paper [8].

3. Results

3.1. Crystal structure

The reflections observed in the neutron diffraction pattern obtained at 300 K (see fig. 3) are characteristic of nuclear scattering for the TiNiSi-type structure. In this pattern at $2\theta = 54°$ a small impurity reflection is observed. At $T = 15$ K a new small magnetic peak due to an impurity appears at $2\theta = 10°$. The TiNiSi-type structure belongs to the Pnma group, sites 4(c) of which x, $\frac{1}{4}$, z; $\bar{x}$, $\frac{3}{4}$, $\bar{z}$; $\frac{1}{2}-x$, $\frac{3}{4}$, $\frac{1}{2}+z$; $\frac{1}{2}+x$, $\frac{1}{4}$, $\frac{1}{2}-z$; are occupied by 4 Tb, 4 Ni and 4 Ge atoms with different values of the x and z parameters. The experimental data were analyzed by the Rietveld profile procedure [9] in which three pairs of (x, z) parameters were subjected to the least-squares calculations. The parameters corresponding to the minimum of disagreement factors are listed in table 1.

The neutron diffraction pattern of DyNiGe obtained at $T = 12$ K has reflections corresponding to the TiNiSi-type structure. The small intensities of these reflections, connected with the large coefficient of absorption of Dy atoms made it impossible to obtain the precise values of position parameters of atoms.

3.2. Magnetic properties

The temperature dependence of the magnetic susceptibility of TbNiGe and DyNiGe exhibits maxima at 18.5 and 4.7 K, respectively (see figs. 1 and 2) which are characteristic of a transition to an antiferromagnetic state. At higher temperatures the magnetic susceptibility is described by the relation $\chi = \chi_0 + C/(T - \vartheta)$. The value of χ_0, the paramagnetic Curie temperature ϑ and the effective magnetic moments μ_{eff} are given in table 2. The values of these parameters are compared with the data in ref. [6].

3.3. Magnetic structure

3.3.1. TbNiGe

A comparison of the room-temperature diagram with the neutron diffraction pattern of TbNiGe measured at low temperatures (below 18 K) shows the presence of additional peaks (see fig. 3) resulting from the onset of magnetic ordering.

Table 1
Crystal structure data for TbNiGe and DyNiGe

Compound	TbNiGe		DyNiGe	
	$T = 35$ K (this work)	$T = 293$ K (from ref. [6])	$T = 12$ K (this work)	$T = 293$ K (from ref. [6])
a [Å]	6.9499(4)	6.922	6.834(3)	6.895
b [Å]	4.2306(3)	4.290	4.197(2)	4.271
c [Å]	7.2813(4)	7.295	7.228(3)	7.280
x_{Tb}	0			
z_{Tb}	0.7071(4)			
x_{Ni}	0.1945(2)			
z_{Ni}	0.0847(3)			
x_{Ge}	0.3055(2)			
z_{Ge}	0.4153(3)			
B_{Tb} [Å^{-2}]	0.51(5)			
$B_{\text{Ni,Ge}}$ [Å^{-2}]	0.58(3)			
R [%]	5.8			

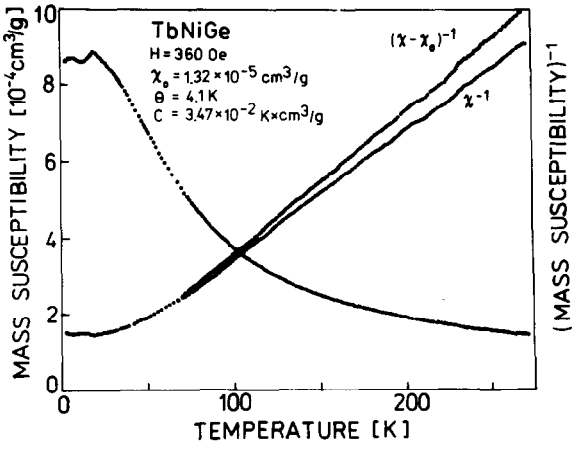

Fig. 1. Temperature dependence of the magnetic susceptibility and the reciprocal susceptibility for TbNiGe.

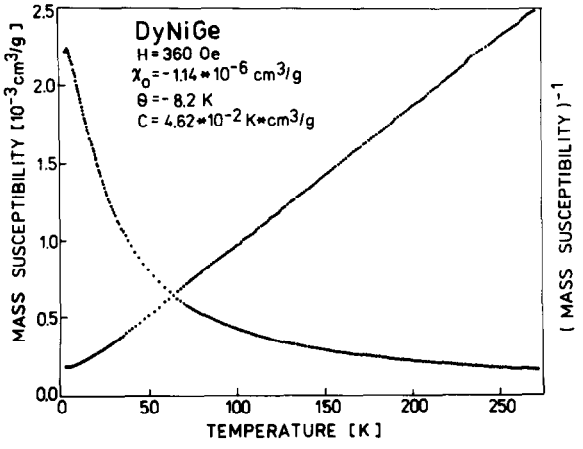

Fig. 2. Temperature dependence of the magnetic susceptibility and the reciprocal susceptibility for DyNiGe.

The magnetic reflections observed in the neutron diffraction pattern at $T = 14.65$ K could be indexed by assuming a magnetic structure with the propagation vector $\boldsymbol{k} = (0.716, 0.309, 0)$.

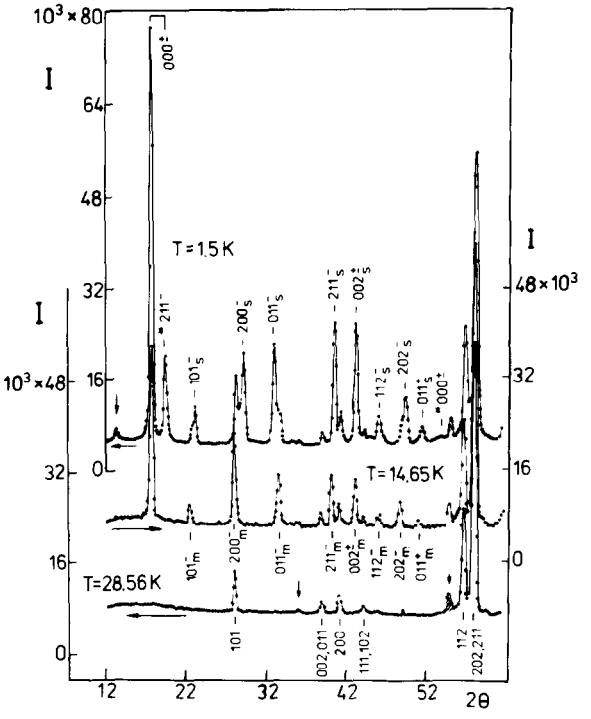

Fig. 3. Neutron diffraction pattern of TbNiGe at 1.5, 14.65 and 28.56 K. Arrows show the peaks corresponding to the impurity phases.

There are four possible types of the magnetic structure: conical spiral, flat spiral, sine modulated or square modulated. The best agreement of the calculated and observed intensities was obtained for a sinusoidally modulated structure. The magnetic moment distribution in such a structure for a νth atom in an nth unit cell is given by the relation

$$\mu_{n\nu} = \hat{x}\mu_\nu^0 \cos(\boldsymbol{k}\cdot\boldsymbol{R}_{n\nu} + \phi_\nu); \qquad (1)$$

Table 2
Magnetic data for TbNiGe and DyNiGe compounds

Compound	T_N [K]	ϑ [K]	μ_{eff} (μ_B/R^{3+})		χ_0 [×10^6 cm^3/g]	Ref.
			exp.	theor.		
TbNiGe	18.5	+4.1	8.97	9.72	13.2	this work
	7	−9	9.45			[6]
DyNiGe	4.7	−8.2	10.42	10.65	1.14	this work
	9	−6	10.40		[6]	

Table 3
Magnetic intensities for TbNiGe. The indices refer to the orthorhombic chemical cell and the reflections $hkl^{\pm}$ are given satellite at $T = 1.5$ and 14.65 K (obs: observed, calc: calculated)

$T = 1.5$ K					$T = 14.65$ K			
hkl	$2\theta_{calc}$	$2\theta_{obs}$	I_{calc}	I_{obs}	$2\theta_{calc}$	$2\theta_{obs}$	I_{calc}	I_{obs}
$000^{\pm}$	17.5	17.5	796.6	788.0	17.73	17.7	359.1	362.2
$*211^{-}$	19.2	19.25	176.2	176.0				
101^{-}	23.0	23.0	65.9	97.6	22.40	22.58	35.5	42.2
200^{-}	29.0	29.0	292.1	287.0	28.0	28.0	170.0	180.3
011^{-}	32.73	32.78	253.3	254.0	33.7	33.7	130.8	134.5
$*200^{-}$	32.87		11.4					
$*220^{-}$	34.0		9.2					
211^{-}	40.33	40.35	281.5	293.5	40.42	40.18	122.0	121.8
101^{+}	41.2	41.15	25.7	25.1	41.54	41.15	12.0	8.0
$002^{\pm}$	43.0	43.0	238.8	296.0	43.0	43.15	115.1	118.5
$*301^{-}$	43.3		0.5					
$*101^{-}$	44.14		2.2					
$*121^{-}$	45.05		0.4					
112^{-}	45.8	45.95	61.0	62.6	46.2	46.2	28.4	28.5
202^{-}	49.25	49.25	172.7	166.8	48.63	48.73	89.4	74.8
011^{+}	51.37	51.35	20.1	60.0	50.68	51.05	27.5	23.8
$*202^{-}$	51.85		13.3					
$*000^{\pm}$	54.35		11.2					
R [%]			7.9				6.9	

μ_ν^0 is the amplitude of the sinusoidal variation of the ν-th atom which for a free R^{3+} ion is gJ; $\hat{x}$ is a unit vector in the direction of the varying moment component; ϕ_ν is the phase angle of the νth moment (in the unit cell); $\boldsymbol{R}_{n\nu}$ is the positional vector of the νth atom in the nth cell; $\boldsymbol{k}$ is the wave vector. The minimum of the reliability factor equals $R_m = 6.9\%$ which corresponds to the situation when the moment is parallel to the a-axis and the phase angle ϕ_ν equals zero.

In the neutron diffraction patterns obtained at $T = 1.5$ K new reflections are observed. Apart from the reflections observed at $T = 14.65$ K, additional reflections (which could be indexed by the propagation vector $\boldsymbol{k}' = (0.68, 0.328, 0)$ and $3\boldsymbol{k}'$) are observed. The new reflections may correspond to the square modulated structure. For both types of the magnetic structure the magnetic moment localized on Tb^{3+} ion is parallel to a-axis and the refined value $9.1\mu_B$ of the magnetic moment of Tb^{3+} ion equals the one for free Tb^{3+} ion ($gJ = 9\mu_B$) within the error limits. The proposed magnetic structures for both phases of TbNiGe are displayed schematically in fig. 4.

Table 3 lists the observed and calculated positions as well as intensities of magnetic reflections for both phases at $T = 1.5$ and 14.65 K. The temperature dependence of some reflections are presented in fig. 5. It follows that:

(1) the temperature dependence of the $(000)^{\pm}$ reflection gives the Néel temperature $T_N = 17.5$ K;
(2) the $*(211)^{-}$ reflection corresponding to $3\boldsymbol{k}'$ wave vector increases with increasing temperature;
(3) the $(101)^{-}$ and $(011)^{-}$ reflections correspond to $\boldsymbol{k}$ and $\boldsymbol{k}'$ wave vectors. The intensities of reflections corresponding to $\boldsymbol{k}'$ decrease with increase in temperature. For $\boldsymbol{k}$ reflections with an increase in temperature the intensities first increase and next decrease. The temperature dependence of both reflection intensities gives the Néel temperature 16.5 K. A very strong hysteresis is observed for this dependence.

An analysis of the neutron diffraction patterns measured at different temperatures allowed the

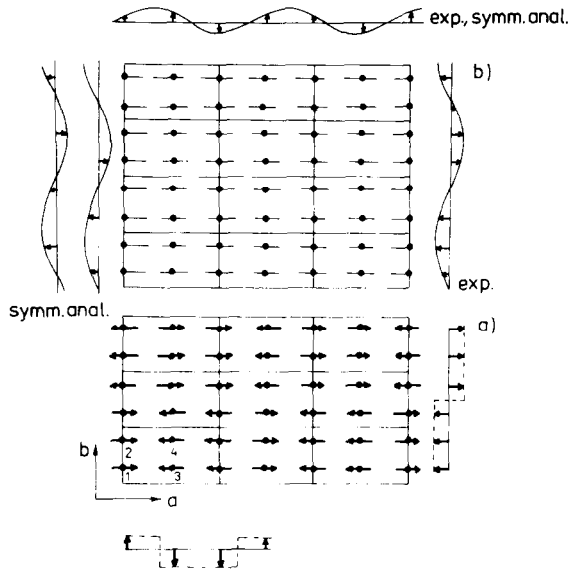

Fig. 4. Schematic representation of the magnetic structures proposed for the low-temperature (a) and high-temperature (b) magnetic phase of TbNiGe. For high-temperature phase, the symmetry analysis (symm. anal.) and neutron diffraction data (exp.) are compared.

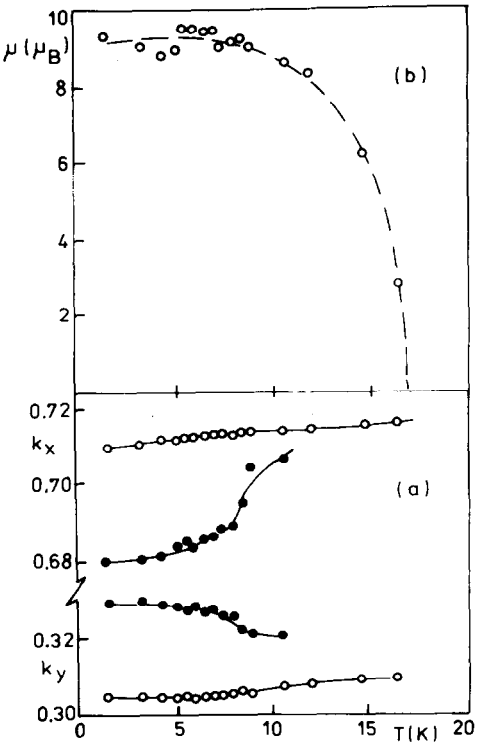

Fig. 6. Temperature dependence, (a) of the component of the wave vector (○ – since modulated, × – square modulated); (b) of the magnetic moment.

determination of the values of the wave vector, k_x and k_y, and the parameters of the magnetic structure. The values of the wave vector, k_x and k_y, are presented in fig. 6a. k_x and k_y corresponding to a sinusoidally modulated structure increase with increasing temperature. A different dependence is observed in the case of k_x and k_y components corresponding to a square modulated structure; the k_x values decrease with increasing temperature whereas the k_y values increase.

Above temperature $T_t = 11.5$ K the reflections corresponding only to the sinusoidally modulated

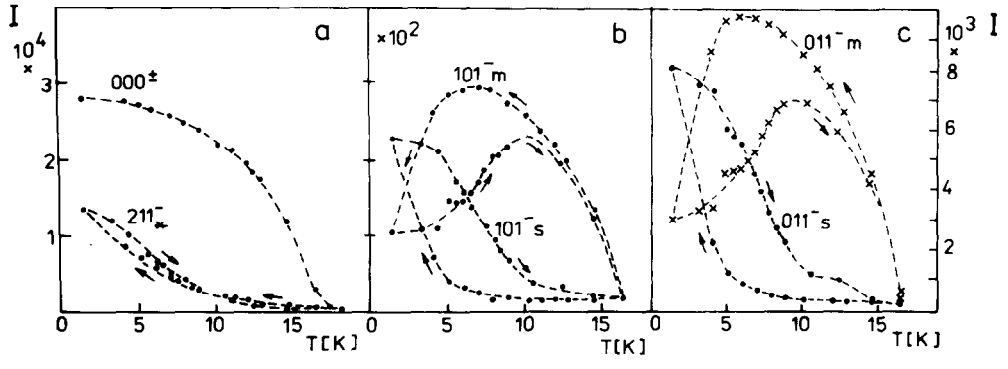

Fig. 5. Temperature dependence of the integrated intensities of $(000)^{\pm}$, 211^{-}, 101^{-}_{m}, 101^{-}_{s}, 011^{-}_{m} and 011^{-}_{s} reflections (m – sine modulated structure, s – square modulated structure).

structure are observed. The analysis of the neutron intensities indicates that the value of the magnetic moment decreases with increasing temperature (see fig. 6b). In the coexistence region the moment values were derived by means of the expression $\mu^2 = \mu_1^2 + \mu_2^2$, where μ_1^2 and μ_2^2 were the moment values of the two phases per unit volume. The value of the magnetic moment localized on the terbium atoms did not change at T_t.

3.3.2. DyNiGe

In the diffraction patterns measured at low temperatures similar reflections to those obtained for TbNiGe are observed. Figure 7 presents between 1.65, 2.5, 3.5 and 12 K.

The magnetic reflection patterns taken at $T = 1.65$ K are indexed by the wave vectors $\boldsymbol{k} = (0.68, 0.32, 0)$ and $3\boldsymbol{k}$, respectively. In the patterns obtained at 2.5 K peaks corresponding to the $\boldsymbol{k}$ and $\boldsymbol{k}'$ wave factors are observed. In the neutron diffraction patterns obtained at 3.5, 4.5 and 5.5 K reflections corresponding to the $\boldsymbol{k}' = (0.71, 0.30, 0)$ wave vector are observed. The temperature dependence of the intensities of the magnetic reflections are shown in fig. 8. This dependence indicates that the Néel temperature is close to 6 K while at about 3 K a change in magnetic structure is observed. The analysis of the position of the magnetic reflections indicate that the value of components of wave vector change at the temperature $T_t = 3$ K (see fig. 9a). The calculation performed for the neutron diffraction pattern obtained at $T = 1.65$ K gives the minimum of the reliability factor ($R_m = 8.1\%$) for the square-modulated structure (see fig. 10a), while for $T = 3.5$ K the minimum of reliability factor corresponds to the cycloidal spiral (see fig. 10b). In the latter case the obtained value of the reliability factor is large ($R_m = 29.2\%$). The sinusoidally modulated structure model gives also a large value of the reliability ($R_m = 43.6\%$). These results indicate that magnetic structure of a high-temperature phase of DyNiGe is complicated and close to a cycloidal spiral.

In both types of magnetic structure the magnetic moments are parallel to the a-axis. At $T = 1.65$ K the magnetic moment equals $7.54\mu_B$ which is smaller than that for free Dy^{3+} ions ($gJ = 10\mu_B$). A comparison of the observed and calculated intensities is given in table 4.

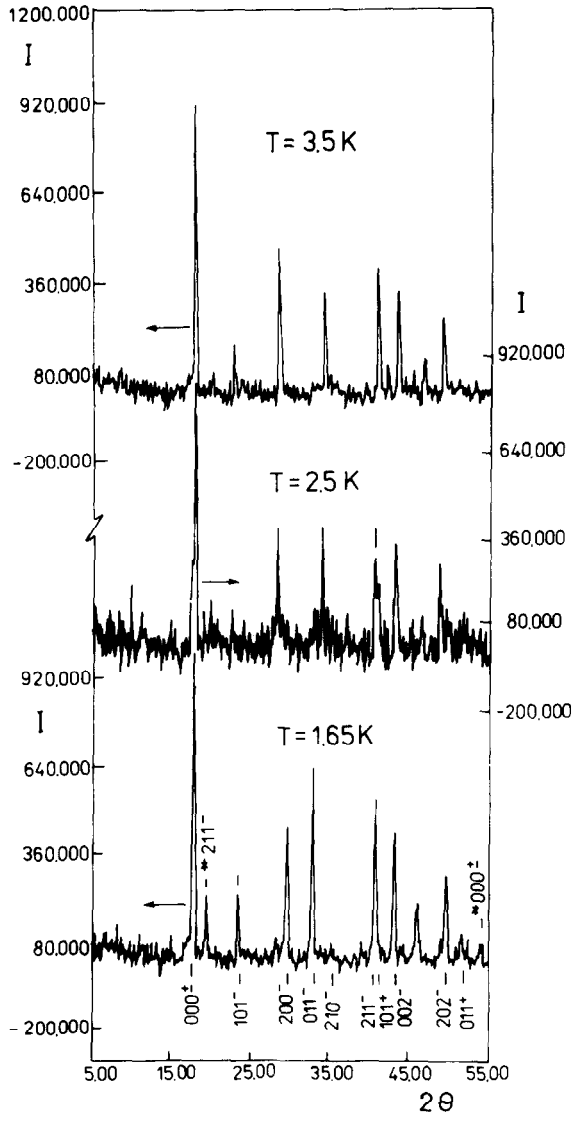

Fig. 7. Neutron differential patterns between 1.65, 2.3, 3.5 and 12 K for DyNiGe.

4. Symmetry analysis

The group-theoretical calculations known as the symmetry analysis method allow the possibility of finding all models of the magnetic struc-

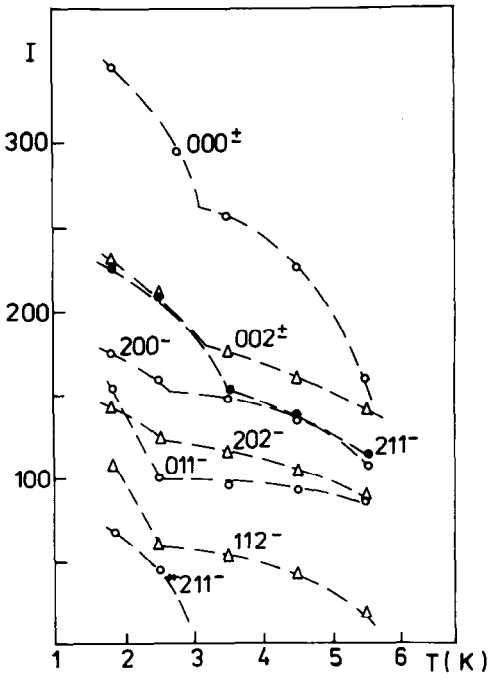

Fig. 8. The temperature dependence of the integrated intensities for DyNiGe.

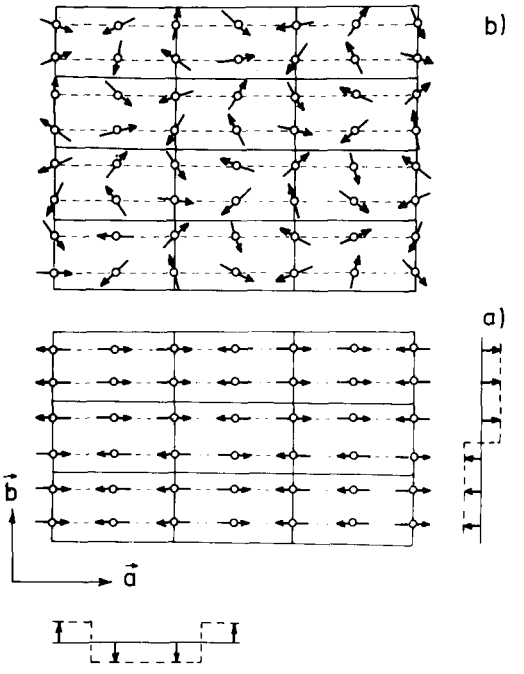

Fig. 10. Schematic representation of the magnetic structures proposed at low temperature (a) and high temperature (b) for DyNiGe.

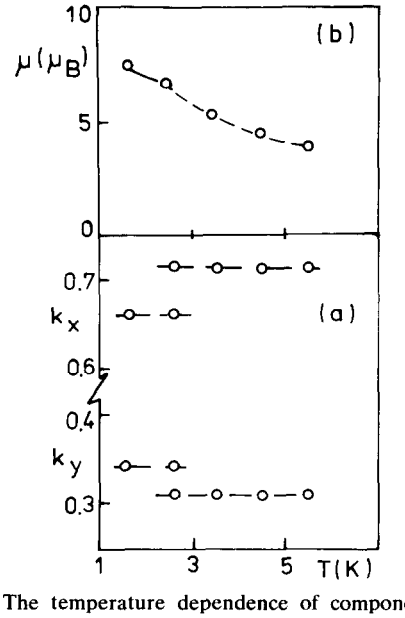

Fig. 9. The temperature dependence of component of the wave vector (a) and magnetic moment (b) for DyNiGe.

tures admitted by paramagnetic phase symmetry after the phase transition. These models, regarded as some axial vector functions determined on a given set of equivalent positions with symmetry of space group G, may be given as the linear combinations of basic vectors of this space group representations:

$$S(r) = \sum_{\nu,\lambda,l} c_{\lambda}^{\nu l} \psi_{\lambda}^{\nu l} \qquad (2)$$

(ν, λ and l number the representation, its dimension and arms of star of k vector respectively).

The results of experiments show, that the TbNiGe magnetic structure at 14.65 K is an incommensurate one with the $k = (0.71, 0.31, 0)$. This vector belongs to the $\{k_5\}$ star of orthorhombic lattice. The sinusoidally modulated and helicoidal structures must be described by modes belonging to two arms of this star k_1 and $k_4 = -k_1$.

Table 4
Magnetic intensities for DyNiGe. The indices refer to the orthorhombic chemical cell and the reflections $hkl^{\pm}$ are given satellite at $T = 1.65$ and 3.5 K (obs: observed, calc: calculated)

$T = 1.65$ K					$T = 3.5$ K			
hkl	$2\theta_{calc}$	$2\theta_{obs}$	I_{calc}	I_{obs}	$2\theta_{calc}$	$2\theta_{obs}$	I_{calc}	I_{obs}
$000^{\pm}$	17.60	17.60	385.61	344.38	17.75	17.75	262.2	253.7
$*211^{-}$	19.3	19.35	69.9	67.8				
101^{-}	23.45	23.45	41.6	51.9	22.6	22.6	35.1	24.3
200^{-}	29.84	29.6	200.3	183.4	28.38	28.25	89.6	147.8
011^{-}	32.4	32.8	197.4	202.8	33.69	34.0	190.1	95.1
$*220^{-}$	32.8		3.7					
$*200^{-}$	34.24		4.5					
211^{-}	40.66	40.0	154.4	160.0	40.6	40.7	107.5	151.3
101^{+}	41.36	41.0	15.2	16.6	42.0	42.0	7.9	8.0
$002^{\pm}$	43.2	43.2	145.0	150.9	43.26	43.3	111.0	175.2
$*121^{-}$	43.56		0.2					
$*112^{-}$	44.36		3.5					
$*101^{-}$	44.78		0.8					
$*301^{-}$	45.17		0.2					
$*011^{-}$	45.9		8.0					
112^{-}	46.04	45.85	50.0	40.0	46.5	46.65	33.7	31.9
202^{-}	49.97	49.85	110.8	121.4	49.94	48.90	73.6	95.8
011^{+}	51.8	51.8	90.5	91.0	51.02	51.0	60.5	61.0
$*202^{-}$	52.95		5.3					
$*020^{-}$	53.6		0.3					
$*000^{\pm}$	54.64		4.4					
$*400^{-}$	55.3		0.3					
R [%]			8.1				29.2	

Table 5
Modes for τ_1 (upper sign) and τ_2 (lower sign) representations $\{k_5\}$ star, D_{2h}^{16} space group, 4(c) positions, without phase displacement between orbitals. The translation by a_1 lattice vector – multiply each spin noted in the table by $\cos(1.42\pi)$, and the translation by a_2 – multiply them by $\cos(0.62\pi)$; $\alpha = 0.71\pi$, $\beta = 0.58\pi$, $\gamma = 0.13\pi$

Atoms in '0' cell		1			2			3			4		
Components of modes		x	y	z	x	y	z	x	y	z	x	y	z
	Ψ_1'	$\overset{+}{+}1$	0	0				$\mp e^{i\alpha}$	0	0			
k_1 1 orb	Ψ_1''	0	$\overset{+}{+}1$	0				0	$\mp e^{i\alpha}$	0			
	Ψ_1'''	0	0	$\overset{+}{+}1$				0	0	$\pm e^{i\alpha}$			
	Ψ_1'				$\overset{+}{+}1$	0	0				$\mp e^{i\alpha}$	0	0
k_1 2 orb	Ψ_1''				0	$\overset{+}{+}1$	0				0	$\mp e^{i\alpha}$	0
	Ψ_1'''				0	0	$\overset{+}{+}1$				0	0	$\pm e^{i\alpha}$
k_4 1 orb	Ψ_4'				$\pm e^{i\gamma}$	0	0				$= e^{-i\beta}$	0	0
	Ψ_4''				0	$\pm e^{i\gamma}$	0				0	$= e^{-i\beta}$	$\overset{+}{0}$
	Ψ_4'''				0	0	$\pm e^{i\gamma}$				0	0	$\overset{+}{+} e^{-i\beta}$
k_4 2 orb	Ψ_4'	$\pm e^{i\gamma}$	0	0				$= e^{-i\beta}$	0	0			
	Ψ_4''	0	$\pm e^{i\gamma}$	0				0	$= e^{-i\beta}$	$\overset{+}{0}$			
	Ψ_4'''	0	0	$\pm e^{i\gamma}$				0	0	$\overset{+}{+} e^{-i\beta}$			

The linear combination of this modes in the form:

$$S_n = \boldsymbol{M}\, e^{i\boldsymbol{k}\cdot\boldsymbol{t}_n} + \boldsymbol{M}^*\, e^{-i\boldsymbol{k}\cdot\boldsymbol{t}_n}$$
$$= 2S_0(\boldsymbol{m}_1 + p\boldsymbol{m}_2)\cos(\boldsymbol{k}\cdot\boldsymbol{t}_n), \quad (3)$$
$$\boldsymbol{M} = (\boldsymbol{m}_1 + p\boldsymbol{m}_2)S_0; \quad \boldsymbol{m}_1\cdot\boldsymbol{m}_2 = 0; \quad \boldsymbol{m}_1^2 = \boldsymbol{m}_2^2;$$

gives the sine modulated structure with magnetic moments in the $\boldsymbol{m}_1$, $\boldsymbol{m}_2$ plane.

The linear combination in the form:

$$S_n = \boldsymbol{M}\, e^{i\boldsymbol{k}\cdot\boldsymbol{t}_n} + \boldsymbol{M}^*\, e^{-i\boldsymbol{k}\cdot\boldsymbol{t}_n}$$
$$= 2S_0(\boldsymbol{m}_1\cos(\boldsymbol{k}\cdot\boldsymbol{t}_n) + p\boldsymbol{m}_2\sin(\boldsymbol{k}\cdot\boldsymbol{t}_n)), \quad (4)$$
$$\boldsymbol{M} = (\boldsymbol{m}_1 + ip\boldsymbol{m}_2)S_0;\ \boldsymbol{m}_1\cdot\boldsymbol{m}_2 = 0;\ \boldsymbol{m}_1^2 = \boldsymbol{m}_2^2;$$

gives the helicoidal ($p = 1$) or elliptic ($p \neq 1$) structure with magnetic moments rotating in $\boldsymbol{m}_1$, $\boldsymbol{m}_2$ plane [19]. As may be seen from formulae (3) and (4) the $\boldsymbol{k}$ and $-\boldsymbol{k}$ modes on the same atom position must be in the same phase.

The symmetry analysis of TbNiGe (DyNiGe) structure gives two orbits of atom positions (in relation to Gk group): 1 and 3 in the first orbit and 2 and 4 in the second one.

Tables 5 and 6 show that the phase displacement $\phi = 0.13\pi$ is required between magnetic moments modulations which are propagated on this orbits independently. If the structure is described as only one modulation, the phase displacement resulting from $\boldsymbol{k}$ vector between positions 1 and 2 equals $\phi = -0.155\pi$. This difference is too small to be noted by experiment.

If the magnetic moments lie on the a-axis, the representation modes must be used for linear combination, and the $(C_1, 0, 0; -C_1, 0, 0)$ order parameter corresponds to the sine modulated structure (TbNiGe), and $(C_1, iC_2, 0; -C_1, iC_2, 0)$ order parameter corresponds to the helical structure (DyNiGe).

For the $\boldsymbol{k}^{\alpha} = (\frac{2}{3}, \frac{1}{3}, 0)$ together with $\boldsymbol{k}' = 3\boldsymbol{k}$, from the symmetry analysis point of view the magnetic structure retains the modulated, no strictly square, character with the commensurable periods in $\boldsymbol{a}_1$ and $\boldsymbol{a}_2$ directions.

5. Discussion

Our investigation indicates that TbNiGe and DyNiGe compounds crystallize in the orthorhombic TiNiSi-type of crystal structure with the space group Pnma. The terbium or dysprosium atoms occupy the 4(c) site.

The magnetic data show that:

1) the value of the Néel temperatures obtained from magnetometric and neutron diffrac-

Table 6

Modes for τ_1 (upper sign) and τ_2 (lower sign) representations, $\{\boldsymbol{k}_5\}$ star D_{2h}^{16} space group, 4(c) positions, with phase displacement between orbits. The translation by $\boldsymbol{a}_1$ lattice vector – multiply each spin noted in the table by $\cos(1.42\pi)$, and the translation by $\boldsymbol{a}_2$ – multiply them by $\cos(0.62\pi)$; $\alpha = 0.71\pi$, $\beta = 0.58\pi$, $\gamma = 0.13\pi$

Atoms in '0' cell		1			2			3			4		
Components of modes		x	y	z	x	y	z	x	y	z	x	y	z
$\boldsymbol{k}_1$ 1 orb	Ψ_1'	± 1	0	0				$\mp e^{i\alpha}$	0	0			
	Ψ_1''	0	± 1	0				0	$\mp e^{i\alpha}$	0			
	Ψ_1'''	0	0	± 1				0	0	$\pm e^{i\alpha}$			
$\boldsymbol{k}_1$ 2 orb	Ψ_1'				$\pm e^{-i\gamma}$	0	0				$\mp e^{i\beta}$	0	0
	Ψ_1''				0	$\pm e^{-i\gamma}$	0				0	$\mp e^{i\beta}$	0
	Ψ_1'''				0	0	$\pm e^{-i\gamma}$				0	0	$\pm e^{i\beta}$
$\boldsymbol{k}_4$ 1 orb	Ψ_4'				$\pm e^{i\gamma}$	0	0				$= e^{-i\beta}$	0	0
	Ψ_4''				0	$\pm e^{i\gamma}$	0				0	$= e^{-i\beta}$	± 0
	Ψ_4'''				0	0	$\pm e^{i\gamma}$				0	0	$\pm e^{-i\beta}$
$\boldsymbol{k}_4$ 2 orb	Ψ_4'	± 1	0	0				$= e^{-i\alpha}$	0	0			
	Ψ_4''	0	± 1	0				0	$= e^{-i\alpha}$	0			
	Ψ_4'''	0	0	± 1				0	0	$\pm e^{-i\alpha}$			

tion data are different. It suggests a strong influence of the magnetic field on the critical temperature of the magnetic ordering.

2) Observed magnetic structures are complicated and they change with a change in temperature. In the case of TbNiGe an anomaly coexistence of two types of the magnetic structures – square and sinusoidally modulated – in a broad temperature range is observed. The coexistence of two types of magnetic structure was observed for some rare-earth compounds, for example monosilicides and monogermanides [10]. In that case the coexistence of collinear and modulated structures is observed over a broad temperature region. In this case the transition between magnetically ordered phases is of the first order. Of similar character is the phase transition at $T_t = 3$ K in DyNiGe.

3) The experimentally determined magnetic structures are in agreement with those proposed by symmetry analysis. The phase displacement given angle ϕ, anticipated by symmetry analysis (mentioned above in section 4), were not detected experimentally (within the limits of error).

The determined magnetic structures of TbNiGe and DyNiGe are similar to those observed in RCu_2 (R = Tb, Dy) [11,12]. RCu_2 compounds form a $CeCu_2$-type crystal structure and the rare-earth sublattice in RCu_2 is exactly the same as that in RNiGe.

The neutron diffraction studies indicate a collinear antiferromagnetic structure at low temperatures. In the case of $TbCu_2$ the magnetic unit cell is triplet to the chemical one while in the case of $DyCu_2$ it is five times greater. With increase in temperature a change to a modulated structure in both compounds is observed [12]. The magnetic moment is parallel to the a-axis.

An antiferromagnetic ordering (including also modulated structure) observed in (Tb, Dy)Cu_2 and (Tb, Dy)NiGe may be explained as due to the competition between the long-range exchange interaction which polarize the conduction electrons and the magneto-crystalline anisotropy caused by the influence of the crystalline electric field on the 4f-electrons.

The RKKY-type exchange interactions favour the long-range oscillatory antiferromagnetic ordering while the magneto-crystalline anisotropy favours uniaxial magnetic ordering. The stability at low temperatures of the magnetic structure of $TbCu_2$ and $DyCu_2$ was calculated by Kimura [13]. A magnetic ordering observed at low temperatures results from the inclusion of higher-order exchange interactions (the biquadratic and a special type of the 4-body interaction). The temperature dependence changes in the magnetic structure are also considered. A modulated structure observed at high temperatures comes from biquadratic exchange interaction between the nearest R^{3+} ions in the neighbouring planes [14].

The comparison of the values of the Néel temperatures for $TbCu_2$ ($T_N = 54$ K) [11], $DyCu_2$ ($T_N = 26.7$ K) [15], TbNiGe ($T_N = 18$ K) and DyNiGe ($T_N = 6$ K) suggests that in the case of RNiGe compounds the magnetic interactions are weaker than in RCu_2 compounds.

The second factor which influences the magnetic ordering is a magnetocrystalline anisotropy due to the crystal field.

The rare-earth site symmetry is C_{2v} and consequently the crystal field Hamiltonian is of the form

$$H_{CF} = \sum_{l,m} \xi_l V_l^m O_l^m, \tag{5}$$

where $l = 2, 4, 6$; m is an even and positive number with values from 0 to l and $\xi = \alpha_J, \beta_J, \gamma_J$ for $l = 2, 4, 6$, respectively. The meaning of the symbols is given in ref. [16].

The above Hamiltonian was derived on the basis of a simple point-charge ionic model of the crystal lattice [16]. The results of the magnetization and susceptibility measurements of $TbCu_2$ and $DyCu_2$ single crystals pointed out that the magneto-crystalline anisotropy attributed to the crystal field plays an important role in the magnetism of these compounds [17].

The observed value of the magnetic moment of Tb atom in TbNiGe is equal to a free ion value for Tb^{3+} ($gJ = 9\mu_B$) within error limits. The large value of magnetic moment indicates that the crystal field of an orthorhombic symmetry acting on the Tb^{3+} ions must lead to the ground state with two very close singlets $\frac{1}{2}(|6\rangle + |-6\rangle)$ and $\frac{1}{2}(|6\rangle - |-6\rangle)$.

In the case of DyNiGe the magnetic moment of Dy atoms is smaller than a free ion value for Dy^{3+} ($gJ = 10\mu_B$). The reduction of the magnetic moment might be due to the crystal electric field and at the same time an effect of hybridization. In both compounds the magnetic moments are parallel to the a-axis. These results indicate that the uniaxial anisotropy is very large.

A crystal field calculation using the point charge model for an orthorhombic crystal [18] indicates that a strong anisotropy is present for terbium atoms and gives the moment direction along the a-axis.

Acknowledgement

This work has been partially supported by the State Committee for Scientific Research in Poland with Grant 2-0083-91-01 and a statutory fund of Academy of Mining and Metallurgy.

References

[1] E. Hovestreydt, N. Engel, K. Klepp, B. Chabot and E. Parthé, J. Less-Common Met. 85 (1982) 247.
[2] D. Mazzone, R. Rossi, R. Marazza and R. Ferro, J. Less-Common Met. 80 (1981) 47.
[3] P. Rogl, in: Handbook on Physics and Chemistry of Rare Earths, vol. 7, eds. K.A. Gschneidner Jr. and L. Eyring (North-Holland, Amsterdam, 1984) chap. 51, p. 1.
[4] E. Parthé and B. Chabot, in: Handbook on the Physics and Chemistry of Rare Earths, vol. 7, eds. K.A. Gschneidner Jr. and L. Eyring (North-Holland, Amsterdam, 1984) chap. 48, p. 113.
[5] A. Szytuła, in: Handbook of Magnetic Materials, vol. 6, ed. K.H.J. Buschow (North-Holland, Amsterdam, 1991) chap. 2, p. 83.
[6] P.A. Kotsanidis, J.K. Yakinthos and E. Gamari-Seale, J. Less-Common Met. 157 (1990) 295.
[7] A. Delapalme, Rapport Interne CEA-CNRS/DPh.G. SDN/LLB/85/59.
[8] A.J. Freeman and J.P. Desclaux, J. Magn. Magn. Mater. 12 (1979) 11.
[9] H.M. Rietveld, J. Appl. Cryst. 2 (1969) 65.
[10] P. Schobinger-Papamantellos and K.H.J. Buschow, J. Magn. Magn. Mater. 62 (1986) 15, 71 (1988) 134; J. Solid State Chem. 70 (1987) 249.
[11] T.O. Brun, G.P. Felcher and J.S. Kouvel, AIP Conf. Proc. 5 (1971) 1376.
[12] B. Lebech, Z. Smetana and V. Šíma, J. Magn. Magn. Mater. 70 (1987) 97.
[13] I. Kimura, J. Magn. Magn. Mater. 52 (1985) 199, 70 (1987) 273.
[14] I. Kimura, J. Magn. Magn. Mater. 86 (1990) 240.
[15] N.H. Luong, J.J.M. Franse and T.D. Hien, J. Magn. Magn. Mater. 50 (1985) 254.
[16] N.T. Hutchings, Solid State Phys. 16 (1964) 227.
[17] Y. Hashimoto, J. Sci. Hiroshima Univ. Ser. A 43 (1979) 157.
[18] V.N. Nguyen, J. Rossat-Mignod and F. Tcheou, Solid State Commun. 17 (1975) 101.
[19] Yu.A. Izyumov and V.E. Naish, J. Magn. Magn. Mater. 12 (1979) 239.
Yu.A. Izyumov, V.E. Naish and V.N. Syromyatnikov, J. Magn. Magn. Mater. 12 (1979) 249.
Yu.A. Izyumov and O.V. Gurin, J. Magn. Magn. Mater. 36 (1983) 226.